Research Article | Vol. 31, No. 11 / 22 May 2023 / Optics Express 18654
Optics EXPRESS

Elimination of surface/subsurface defects on additively manufactured AlSi10Mg mirrors through nano-second laser irradiation

CHEN LIU,[1,2] ZHIYU ZHANG,[1,*] XUEFENG ZENG,[1] XU YANG,[3] WEIJIE DENG,[1] AND XUEJUN ZHANG[1,2]

[1] *Changchun Institute of Optics, Fine Mechanics and Physics, Chinese Academy of Sciences, Changchun, Jilin 130033, China*
[2] *University of Chinese Academy of Sciences, Beijing 100049, China*
[3] *Jilin University, Changchun, Jilin 130025, China*
[*] *zhangzhiyu@ciomp.ac.cn*

Abstract: Metal mirrors have attracted increasing attention for satisfying the growing demands for high-performance optics in airborne and spaceborne remote sensing systems. Additive manufacturing has enabled the development of metal mirrors with reduced weight and improved strength. AlSi10Mg is the most widely used metal for additive manufacturing. Diamond cutting is an effective method for obtaining nanometer-scale surface roughness. However, the surface/subsurface defects of additively manufactured AlSi10Mg deteriorate the surface roughness. Conventionally, AlSi10Mg mirrors used in near-infrared and visible systems are plated with NiP layers to improve the surface polishing performance; however, this leads to the bimetallic bending because of the different coefficients of thermal expansion between the NiP layers and AlSi10Mg blanks. In this study, a method of nanosecond-pulsed laser irradiation is proposed to eliminate the surface/subsurface defects of AlSi10Mg. The microscopic pores, unmolten particles and two-phase microstructure of the mirror surface were eliminated. The mirror surface exhibited better polishing performance, and it could be smoothly polished to a nanometer-scale surface roughness. The mirror exhibits strong temperature stability owing to the elimination of the bimetallic bending caused by the NiP layers. It is expected that the mirror surface fabricated in this study can satisfy the requirements for near-infrared or even visible applications.

1. Introduction

Optical mirrors are key components in modern remote sensing systems for airborne and spaceborne applications. Metal mirrors, especially aluminum alloy mirrors, are promisingly used in the applications due to their good processing performance and low material cost [1,2]. Additive manufacturing is a layer-by-layer processing technology that promotes the formation of complex structures which cannot be achieved by subtractive machining [3–6]. Additive manufacturing technology has important prospects for fabricating metal mirrors [7–9].

AlSi10Mg is a typical aluminum alloy material used in the additive manufacturing of metal mirrors [10,11]. AlSi10Mg alloy has the characteristics of light weight, less porosity and low cost, compared to other materials such as Ti6Al4V, stainless steel and Inconel. With the rapid development of additive manufacturing, it is possible to fabricate a closed-back mirror with complex internal structures, such as lattice structures, arches, and periodic or topology-optimized structures, to further improve the specific stiffness [12,13].

Diamond cutting is an effective method for additively manufactured AlSi10Mg to achieve mirror surfaces [14–16]. However, the layer-by-layer building process typically used in additive manufacturing leads to forming internal pores or void defects. After diamond cutting, the internal

#491959 https://doi.org/10.1364/OE.491959
Journal © 2023 Received 29 Mar 2023; revised 30 Apr 2023; accepted 2 May 2023; published 18 May 2023

Optics EXPRESS

pores or void defects, which are randomly distributed in the additively manufactured AlSi10Mg mirrors, are exposed on the surface, resulting in surface micropit defects. For example, Hilpert et al. obtained a surface roughness of Sa 14 nm by diamond cutting on an additively manufactured AlSi12 mirror [17]. AlSi12 is also commonly used for additive manufacturing, and has similar defects such as unmolten particles and microscopic pores. The surface defects of AlSi12 or AlSi10Mg significantly affect the reflectivity of the mirrors as they cause surface scattering at the near-infrared and visible wavelengths.

However, it is well known that the surface roughness of optical mirrors after diamond cutting can be improved through chemical mechanical polishing. However, AlSi10Mg has a typical two-phase microstructure; therefore, it is difficult to obtain smooth surfaces from two-phase materials because of physical and chemical differences in the phase and orientation. Herzog et al. reported that additively manufactured AlSi10Mg mirror after pad polishing had a surface roughness of Ra 16 nm. This fully shows that the grain boundary step worsens the polishing performance and the surface roughness of AlSi10Mg in chemical mechanical polishing [18,19].

Currently, the challenge associated with the additive manufacturing of optical mirrors is achieving damage-free surfaces with a nanometer roughness. Mirrors in near-infrared and visible systems are often deposited with NiP layers to improve polishing performance. For example, Yan et al. and Hilpert et al. deposited AlSi10Mg with NiP layers, and reported a surface roughness Ra < 1 nm after chemical mechanical polishing [20,21]. However, the thermal expansion coefficients of AlSi10Mg mirror bodies and NiP layers are quite different. This destroys the temperature stability of the optical mirrors (bimetallic bending) [22].

In recent years, laser polishing has been reported to improve the surface quality of various metals [23,24]. To the best of our knowledge, the laser polishing of additively manufactured workpieces in previous studies mainly focused on as-built surfaces with the use of a high-power continuous laser, which reduced the surface roughness from tens of microns to several microns. For example, Hassanin et al. used a CO_2 laser to polish the AlSi10Mg blank. The as-built surface roughness Ra was approximately 20 µm; after laser polishing, it was reduced to 7 µm [25]. Zhang et al. used a continuous-wave fiber laser to polish a AlSi10Mg blank, and obtained the best surface roughness Sa of 3 µm [26]. Owing to the high laser energy density, the surface roughness is still on the order of microns after laser polishing, which is far from the nanometer level requirement for near-infrared and visible mirrors.

Therefore, eliminating of surface/subsurface defects of AlSi10Mg mirrors without causing bimetallic bending is important. In this study, in contrast to the laser polishing of as-built surfaces using high-power continuous lasers, the modification of the diamond cutting surface with a low-energy nanosecond-pulsed laser was performed to generate a thin modified layer with a thickness of only several microns on the mirror surface. Because the micropit defects and two-phase microstructure are eliminated after laser modification, the mirror shows better polishing performance and can be smoothly polished to a nanometer-scale surface roughness. It is expected that the mirror surfaces fabricated in this study can satisfy the requirements for near-infrared or even visible applications.

2. Material and methods

2.1. Material

The material of the mirror blanks was gas-atomized AlSi10Mg powder supplied by BAM, Ltd.

The shape and size distributions of AlSi10Mg powder are of technological importance for the final built products. Figure 1 shows a scanning electron microscope (SEM) image of the AlSi10Mg powder used in the additive manufacturing. The vast majority of particles have a spherical or nearly spherical shape. The particle size is in the range of 20–60 µm in diameter with a mean size of 40 µm, which is beneficial for increasing the density of the workpieces and avoiding element segregation and shrinkage porosity.

Optics EXPRESS

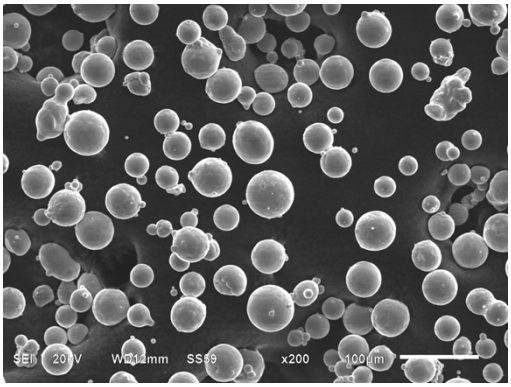

Fig. 1. SEM image of the AlSi10Mg powder.

Selective laser melting (SLM) is a typical additive manufacturing technology that is primarily used for metal forming. The SLM was performed using an FS271M system (laser-powder-bed fusion) with a Yb-fiber laser. A schematic of SLM is shown in Fig. 2. The powder was fed into the building chamber through the roller. For each layer, the laser melts, the workpiece is formed by one layer, and the corresponding piston moves down to the next layer. All workpieces were fabricated with a laser power of 370 W, a scan speed of 1300 mm/s, and a hatch distance of 80 μm. The forming process was carried out in an argon atmosphere with an oxygen mass fraction of less than 0.1%.

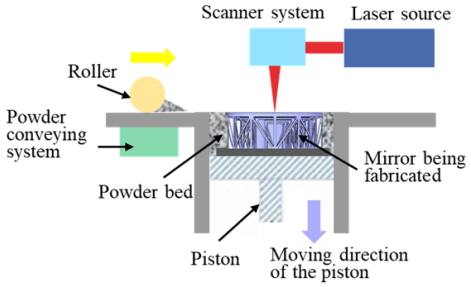

Fig. 2. Schematic of the SLM.

After forming, the hot isostatic pressing was used to reduce the volume porosity of the additively manufactured workpieces. Figure 3 shows the schematic of the hot isostatic pressing. This process requires the workpieces to be placed in a heat-treatment furnace at a temperature of ~510 °C and pressure of ~110 MPa. It was also maintained for approximately 2 hours, after which the workpiece was cooled in the furnace. After hot isostatic pressing, the volume porosities of the additively manufactured workpieces were significantly reduced [27–30].

2.2. *Diamond cutting*

After hot isostatic pressing, diamond cutting was performed using the parameters listed in Table 1. After diamond cutting, the surface topographies were investigated using a laser scanning confocal microscope. Surface roughness was measured using a 3D optical surface profiler (NewView 9000, ZYGO). As mentioned previously, internal micropores were exposed on the surface to form micropits. This process is illustrated in Fig. 4.

Optics EXPRESS

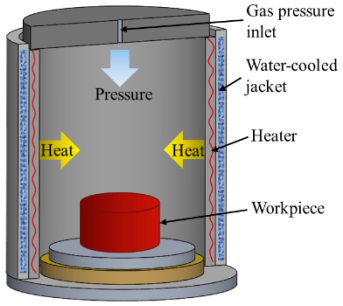

Fig. 3. Schematic of the hot isostatic pressing.

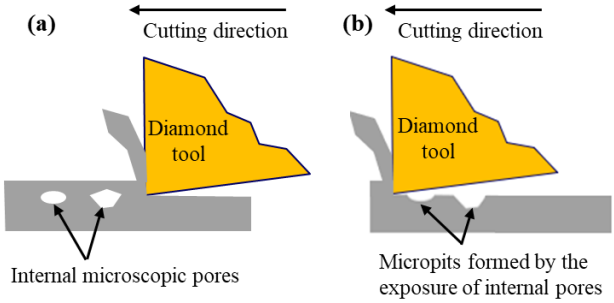

Fig. 4. Schematic of micropits formed by exposure of internal micropores: (a) before and (b) after cutting.

Table 1. Cutting parameters in diamond cutting

Parameter name	Parameter setting
Cutting tool	Single-crystal diamond tool
Tool nose radius	1 mm
Rake angle	0°
Relief angle	10°
Feed rates	0.5, 1, 2, 5, 10 μm/rev
Speed of the spindle	1000 rev/min
Depth of cut	2 μm

2.3. Laser surface modification

A nanosecond-pulse laser machining system (EP30-G8, Changchun New Industries Optoelectronics Technology Co., Ltd., China) was used for the laser surface modification. The main parameters of the laser machining system are listed in Table 2. The laser has a wavelength of 532 nm and a typical pulse width of 50 ns. The laser repetition frequency was set at 60 kHz.

Figure 5 shows the scanning system of the laser beam during irradiation. The beam has a Gaussian energy density distribution. A telecentric f-theta objective lens is used to focus the beam with a nominal beam diameter of 80 μm. The system employs two galvanometer mirrors to achieve two-dimensional scanning. In one scan, the pulse interval along the scanning direction is changed by adjusting the scanning speed; hence, the scanning speed determines the pulse interval. After one scan, the galvanometer mirror system directs the laser to the next scan by a scan pitch; hence, the scan pitch determines the beam overlap ratio.

Optics EXPRESS

Table 2. Main parameters of the laser machining system and laser irradiation conditions

Items	Parameter
Laser type	Nanosecond pulsed laser
Wavelength	532 nm
Pulse width	50 ns
Repetition frequency	60 kHz
Nominal beam diameter	80 μm
Scanning speeds	200–1200 mm/s
Scan pitches	4–40 μm
Average laser powers	3–13 W
Environment	In air at ambient temperature

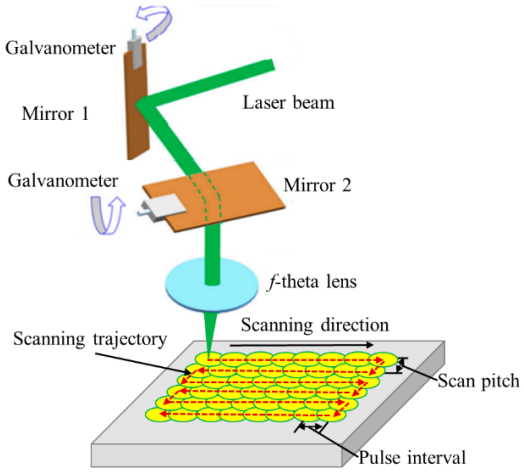

Fig. 5. Schematic of the laser scanning system.

The laser irradiation conditions are also listed in Table 2. The following three-step optimization process was performed. First, the effects of scanning speeds ranging from 200 to 1200 mm/s, corresponding to the pulse intervals of 3.3 to 20.0 μm, on the surface roughness were investigated. Second, the effects of scan pitches from 4 to 40 μm, corresponding to beam overlap ratios of 95 to 50%, were investigated at the optimal scanning speed. Third, with the optimal scanning speed and scan pitch, the average powers from 3 to 13 W were further investigated. All laser irradiations were conducted in air at ambient temperature (~300 K).

2.4. Chemical mechanical polishing

After the laser surface modification, residual tool marks and laser scanning tracks on the mirror surface were evident. Chemical mechanical polishing was applied to further improve surface roughness. As shown in Fig. 6, the polishing experiments were performed on a computer-controlled optical surfacing polishing robot arm. To select the optimal polishing parameters, many types of polishing operations were tested, and SiO_2 polishing powder with a moderate hardness polishing cloth under alkaline conditions was applied. The optimal chemical mechanical polishing parameters are listed in Table 3.

Optics EXPRESS

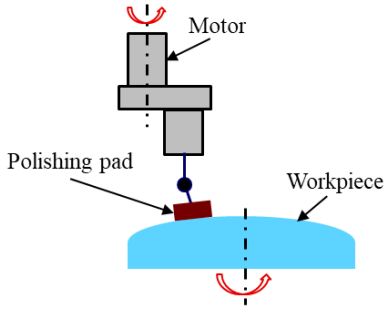

Fig. 6. Schematic of the chemical mechanical polishing.

Table 3. Parameters in the chemical mechanical polishing

Parameter name	Parameter setting
Abrasive	SiO_2
Abrasive particle size	100 nm
Chemical mechanical polishing tool	Polyurethane pad
Pressure	2.5 kPa
pH	9

3. Results and discussion

3.1. Surface roughness after diamond cutting

After each diamond cutting, the surface roughness Sa (arithmetic average roughness) were measured at eight random points. The Sa is calculated using Eq. (1):

$$S_a = \frac{1}{A}\int_A \int |Z(x,y)|\, dxdy. \tag{1}$$

where A implies that the integration is performed over the area of measurement and $Z(x, y)$ is the function representing the height of the surface relative to the best fitting plane. In order to investigate the diamond cutting mechanism, the theoretical surface roughness values Rt (peak to valley roughness) corresponding to the five cuttings are also presented in Fig. 7. The Rt is calculated using Eq. (2) [31],

$$R_t \approx \frac{f^2}{8R}. \tag{2}$$

where f is the feed rate per revolution, and R is the radius of the tool edge.

Figure 7 listed out the comparison of Rt and Sa. As the feed rate decreases, the Rt gradually decrease while the Sa are distributed between 5 and 6 nm. It is concluded that when the feed rates are less than 10 µm/rev, the surface/subsurface defects, such as micropits and the two-phase microstructure, significantly dominate the measured surface roughness. If the feed rates are larger than 10 µm/rev, the surface roughness will be dominated by the residual height of the tool marks, and became more in line with Eq. (2).

3.2. Laser surface modification

3.2.1. Effects of scanning speeds

Laser modification experiments were performed on the diamond cutting surfaces with the feed rate was 5 µm/rev as described in Section 3.1. The average laser power and scan pitch were

Optics EXPRESS

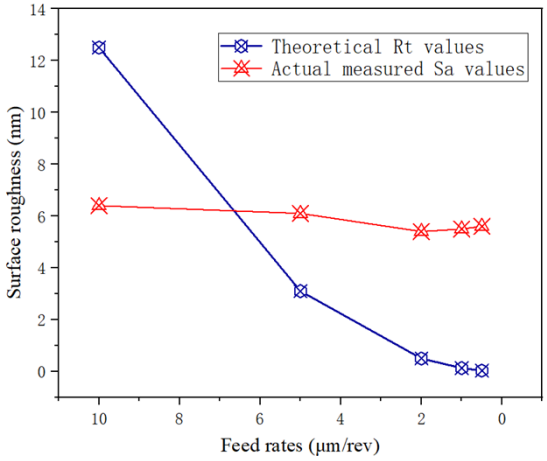

Fig. 7. Theoretical and actual measured surface roughness after each cutting.

set to 7 W and 40 μm, respectively. The scanning speeds were set to 200, 400, 600, 800, 1000, and 1200 mm/s. The surface roughness values at different scanning speeds are shown in Fig. 8. When the scanning speeds were increased from 200 to 800 mm/s, the surface was significantly improved from 26 to 10 nm. When the scanning speeds are further increased to more than 1200 mm/s, the surface roughness will keep at 10–11 nm. A similar phenomenon can also be observed in the surface morphologies as shown in Fig. 9. The undulations of (a), (b) and (c) are relatively larger, and their surface roughness values are larger than those in (d), (e), and (f).

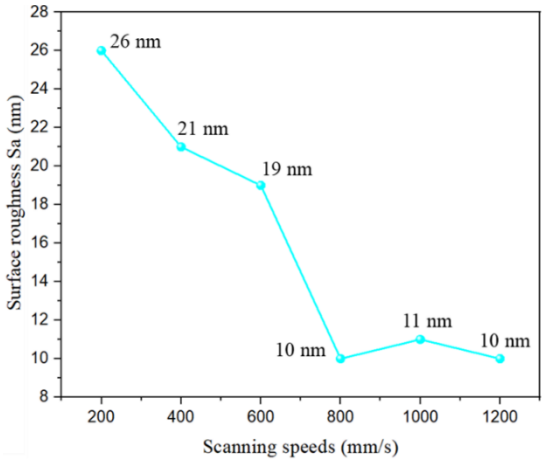

Fig. 8. Surface roughness Sa values at different scanning speeds.

The scanning speeds also affect the thickness of the laser modified layer. Lower scanning speeds resulted in more pulses irradiated on the surface. Thus, thicker modified layers conducive to subsequent polishing were obtained. Although the surface roughness is similar, the thickness of the modified layer at 800 mm/s is larger than those at 1000 and 1200 mm/s, due to more laser pulses irradiating on the material surface. Therefore, the optimal scanning speed was 800 mm/s, which resulted in the best surface roughness and a sufficient thickness of the modified layer.

Optics EXPRESS

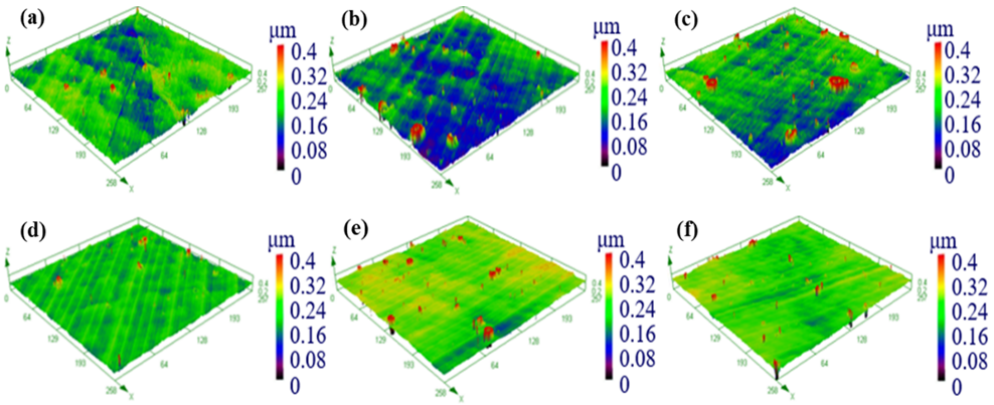

Fig. 9. Surface morphologies at different scanning speeds: (a) 200 mm/s; (b) 400 mm/s; (c) 600 mm/s; (d) 800 mm/s; (e) 1000 mm/s; (f) 1200 mm/s.

3.2.2. Effects of scan pitches

Based on the optimal scanning speed of 800 mm/s, the effects of the scan pitches of 4, 8, 16, 24, 32, and 40 μm were investigated. The scan pitches affect the laser beam overlap ratios. Because the spot diameter is 80 μm, when the scan pitches are too large, inadequately treated areas exist in the middle of the adjacent scanning. As a result, the scan pitches from 4 to 40 μm corresponding to the laser beam overlap ratios ranging from 95% to 50% were applied.

The surface roughness results obtained are shown in Fig. 10. With the increase in the scan pitches, the surface roughness values first decreased and then increased. The best Sa value of 8 nm was obtained at the scan pitch of 24 μm. The surface morphologies are shown in Fig. 11. The surface was relatively smooth at the scan pitch of 24 μm, while bumps and grooves were observed at the other pitches. At the scan pitch of 4 μm, large bumps were observed, which were attributed to intense melting.

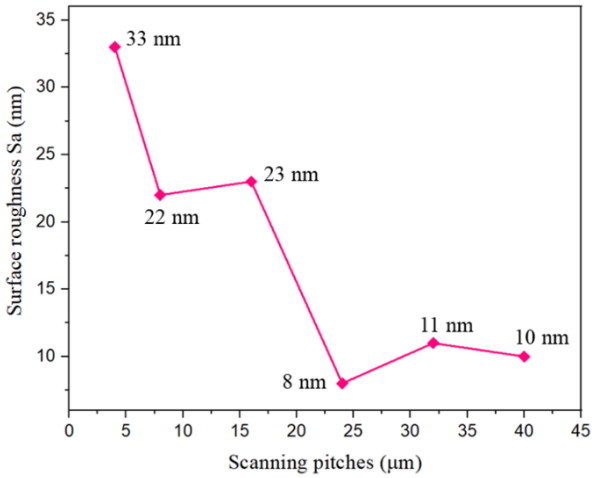

Fig. 10. Surface roughness Sa values at different scan pitches.

After laser irradiation, laser scanning traces were widely distributed on the surface of the irradiated workpieces in Fig. 11(a)–(e). However, some deep tool marks in Fig. 11(f) still existed due to the shallow melting layer.

Optics EXPRESS

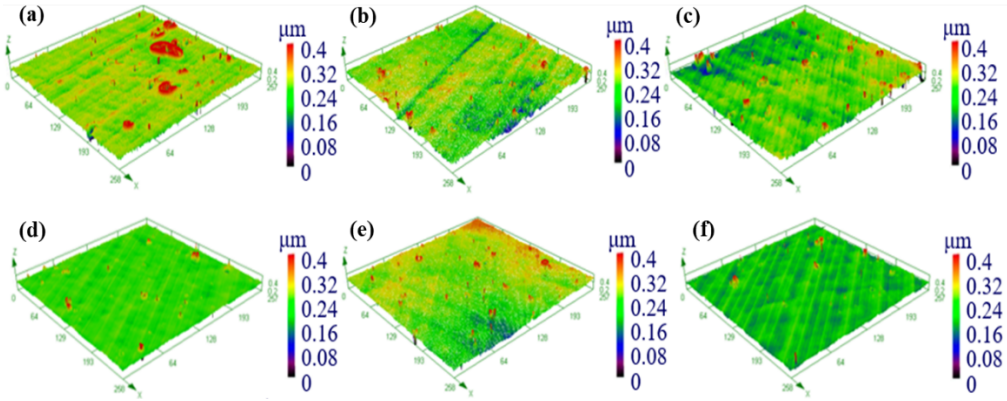

Fig. 11. Surface morphologies at different scan pitches: (a) 4 μm; (b) 8 μm; (c) 16 μm; (d) 24 μm; (e) 32 μm; (f) 40 μm.

3.2.3. Effects of average laser powers

Based on an optimal scanning speed of 800 mm/s and a scan pitch of 24 μm, the effects of the average laser powers of 3, 5, 7, 9, 11, and 13 W were investigated. The surface roughness results obtained are shown in Fig. 12. The surface roughness gradually increased as the average laser powers were gradually increased. The optimal surface roughness was approximately 6 nm at an average laser power of 5 W. Because the experiments were performed on the diamond cutting surfaces with the initial surface roughness of 6 nm, it is concluded that the laser surface modification did not affect the surface roughness under the above-mentioned irradiation conditions. The surface roughness was the same as that of the diamond cutting surface. The surface morphologies are shown in Fig. 13. The surfaces were relatively smooth when the average laser powers were less than 5 W, whereas bumps or holes were generated at the average laser powers greater than 7 W. Evidently, many holes were generated at the average laser power of 13 W.

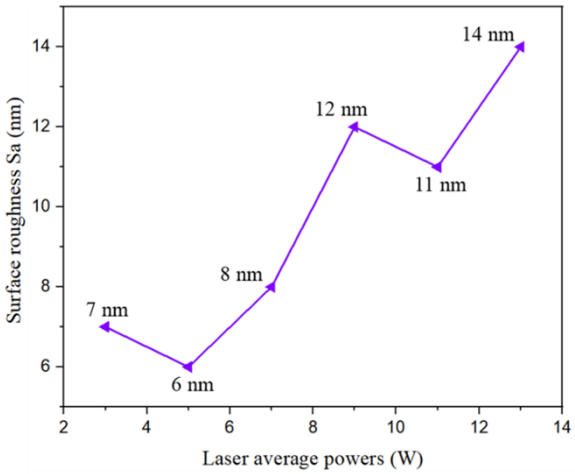

Fig. 12. Surface roughness Sa values at different average laser powers.

Optics EXPRESS

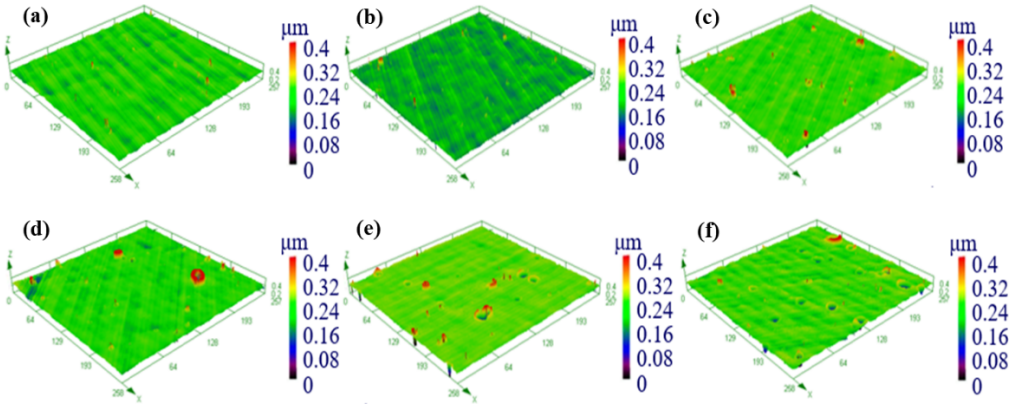

Fig. 13. Surface morphologies at different average powers: (a) 3 W; (b) 5 W; (c) 7 W; (d) 9 W; (e) 11 W; (f) 13 W.

3.3. *Chemical mechanical polishing without laser surface modification*

The chemical mechanical polishing results for the as-built surface are shown in Fig. 14. Evidently, the surface roughness values decreased to a certain extent, indicating that chemical mechanical polishing at the initial stage had a smoothing effect on the tool marks and burrs generated by cutting. The minimum averaged Sa value of 4.6 nm was obtained after 40 minutes of chemical mechanical polishing. As the chemical mechanical polishing time increased, the surface roughness deteriorated. This is because AlSi10Mg is a two-phase material. The hardness of the aluminum and the silicon phases are different, and the removal amounts in polishing are also different. After 40 minutes, increasing the chemical mechanical polishing time resulted in microsteps between the aluminum phase and silicon phase, and the microsteps worsened the surface roughness.

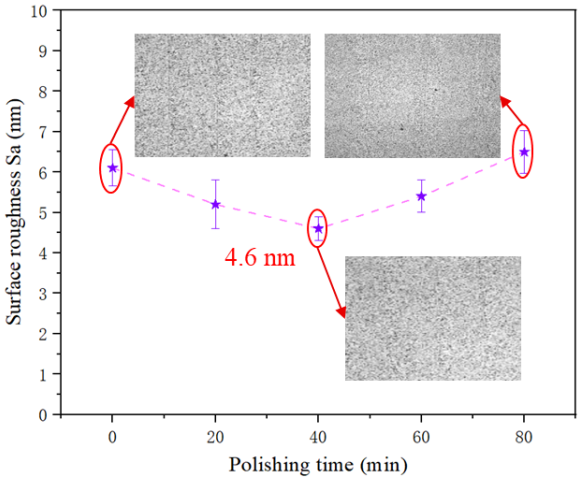

Fig. 14. As-built surface roughness evolution during chemical mechanical polishing.

Optics EXPRESS

3.4. Chemical mechanical polishing with laser surface modification

The chemical mechanical polishing and surface roughness measurement methods after laser modification were the same as those described above. After the laser modification, eight points were measured, and their surface roughness distributions are shown in Fig. 15. The average Sa value is 6.1 nm. According to the SEM images after diamond cutting shown in Fig. 16, it is evident that many unmolten particles and microscopic pores are distributed on the unmodified surface. However, after laser modification, the former defects were eliminated and a uniform surface was obtained. After chemical mechanical polishing, the results were averaged and shown in Fig. 17. After 40 minutes of polishing, the averaged surface roughness value is 3.7 nm, which is approximately 1 nm better than that of the unmodified one.

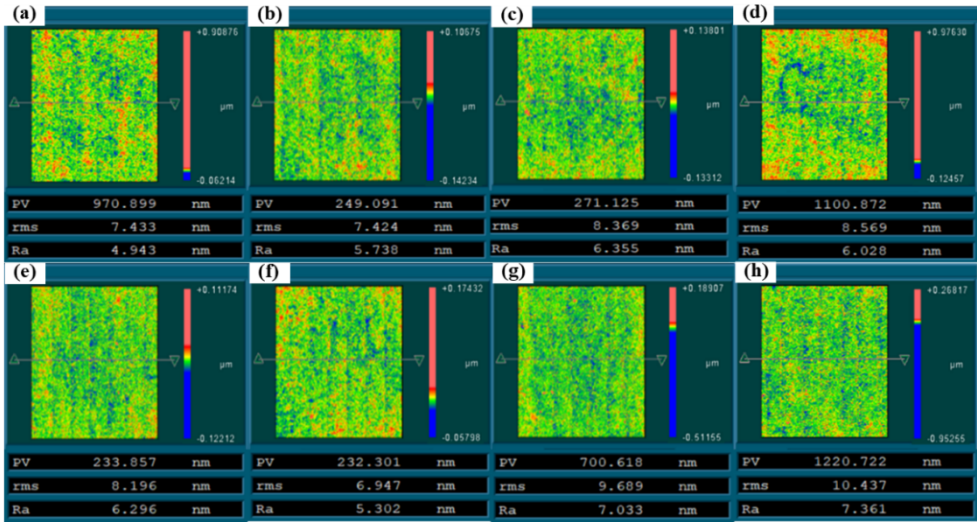

Fig. 15. Roughness results after laser modification: (a)−(h) Point 1−8.

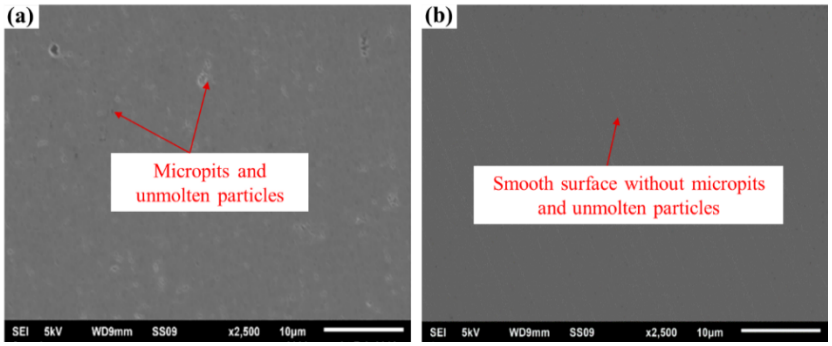

Fig. 16. SEM images of the workpiece surfaces: (a) after diamond cutting; (b) diamond-cut surface after modification.

3.5. Mechanism of polishing performance improvement

To validate the results of the surface roughness analyses, an additional workpiece was laser-modified under the same conditions to ascertain the thickness of the modified layer through SEM observation. Figure 18 shows the changes of the cross-sectional microstructures before and

Optics EXPRESS

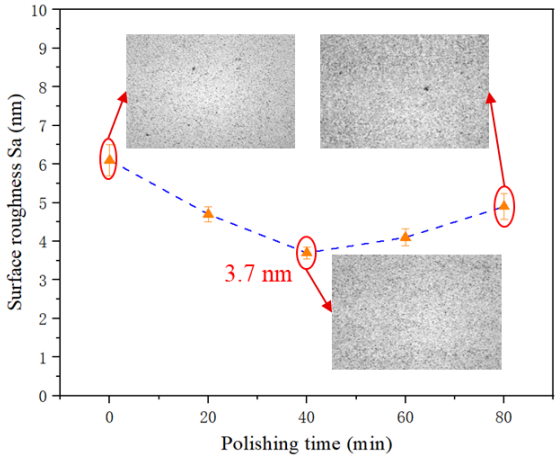

Fig. 17. Roughness evolution during chemical mechanical polishing of laser modified surface.

after laser surface modification. Evidently, the modified layer becomes more uniform, and the micropits or voids are eliminated. The depth of the modified layer is estimated as 7.8 µm. This observation reveals that the repair of surface/subsurface defects is the dominant laser material interaction regime when performing surface modification with a nanosecond pulsed laser with a lower energy density.

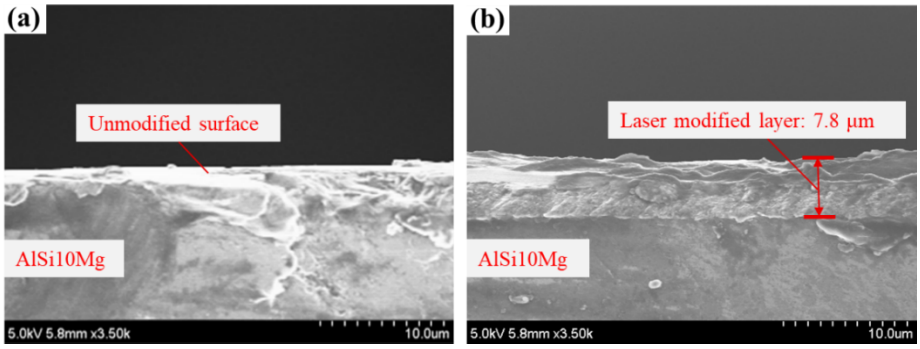

Fig. 18. SEM images from sectional view: (a) after diamond cutting; (b) diamond-cut surface after laser modification.

To investigate the possible elemental changes on the surface caused by laser irradiation, the contents of the elements in the sample before and after laser irradiation were measured using energy-dispersive X-ray spectroscopy (EDX) (EDAX Genesis). Figure 19 shows the EDX spectra of the workpiece surfaces before and after laser irradiation. The major elements on the surface are Al, Si, and O. Furthermore, the O content of the modified surface increased from 1% to 2.33%, indicating the oxidation of aluminum to alumina on the laser-irradiated surface.

During further investigation, the surface hardness on the as-built and laser-irradiated surfaces was also characterized by a nanoindentation instrument (DUH-211, Shimadzu, Japan) equipped with standard data processing software based on the Oliver-Pharr (OP) method [32]. During nanoindentation testing, a pyramidal diamond indenter with an angle of 115° between the ridge and face (pyramidal indenter, Tokyo Diamond Tools MFG. Co., Ltd., Japan) was used, and the indentation load and loading rate were 100 mN and 10 mN/s, respectively. The load-depth

Optics EXPRESS

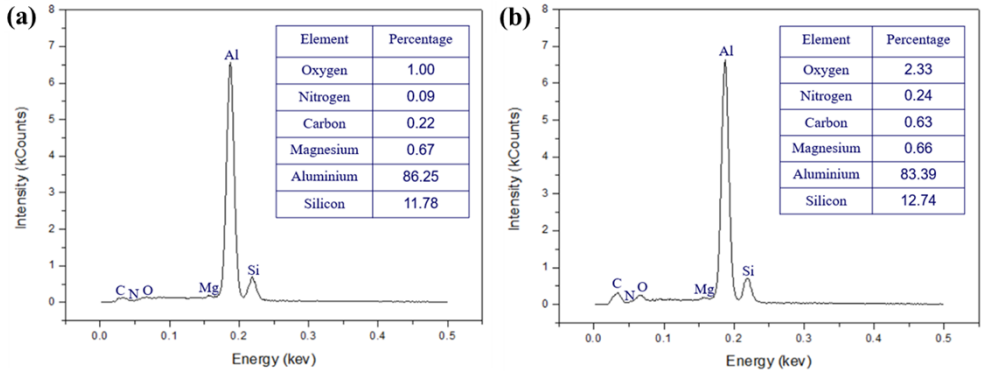

Fig. 19. Energy-dispersive X-ray spectroscopy results: (a) unmodified and (b) modified surface.

curves of the unmodified and the modified surfaces are shown in Fig. 20. The shapes of the two curves are similar, and the maximum force and maximum depth are close, showing similar mechanical properties. Figure 21 shows a comparison of the hardness. After laser modification, the average hardness of the modified layer was 1.56 GPa, whereas that of the unmodified surface was 1.64 GPa. The hardness of the modified layer exhibits a slight decrease under the current laser modification parameters. The nanoindentation results are consistent with the results obtained by EDX. Therefore, there is no significant changes in the surface hardness after laser modification.

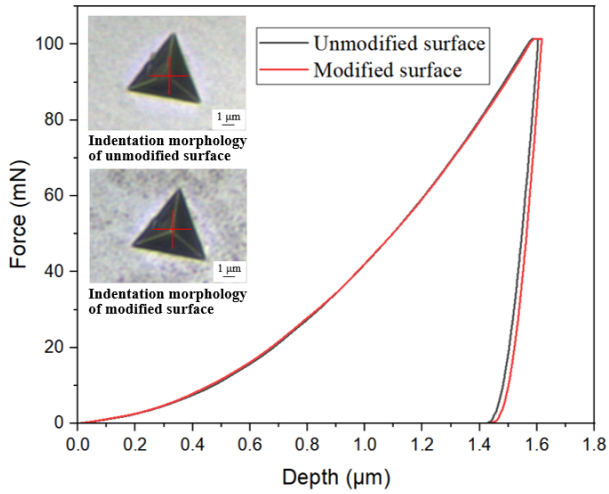

Fig. 20. Load-depth curves of the unmodified and the modified surfaces.

Based on the above analyses, schematics of laser surface modification and polishing performance improvement are shown in Figs. 22 and 23, respectively. Compared with the original two-phase structure, the microscopic pores and unmolten particles were eliminated after laser irradiation. On the surface of the laser modified layer, there is little difference in the depth of the polishing abrasive entry which is prone to form a relatively smooth surface. Grain boundary microsteps between the two phases can also be observed during the as-built chemical mechanical polishing.

Optics EXPRESS

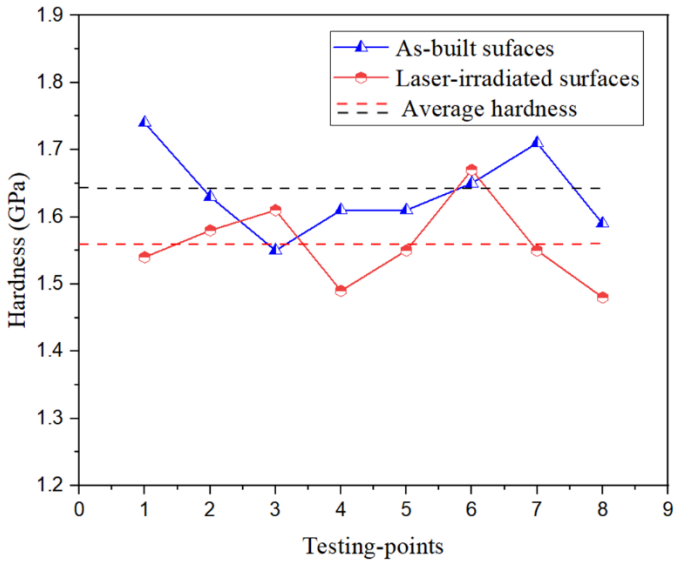

Fig. 21. The surface hardness of the as-built and laser-irradiated surfaces.

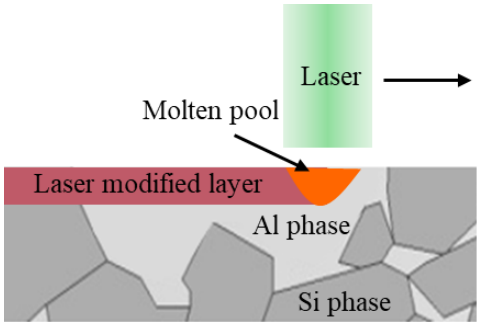

Fig. 22. Schematic of laser surface modification.

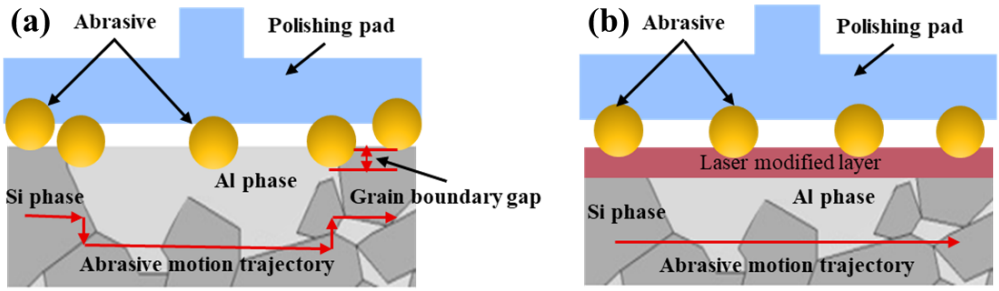

Fig. 23. Mechanisms of chemical mechanical polishing: (a) unmodified surface, (b) modified surface.

Optics EXPRESS

4. Conclusions

In this study, the surface roughness evolution of the additively manufactured AlSi10Mg mirrors was investigated by diamond cutting, surface laser irradiation and chemical mechanical polishing. The following conclusions are drawn from the experiments and analyses:

1. A large number of pores and unmolten particles were distributed inside the as-built AlSi10Mg mirrors. After diamond cutting, relatively large micropits could be observed. The minimum surface roughness Sa value of the mirror was 5−6 nm.

2. After chemical mechanical polishing, the surface roughness value of the additively manufactured mirror was slightly reduced to 4.6 nm. When chemical mechanical polishing was performed further, the value increased owing to the two-phase structure.

3. Laser modification is an effective method to change the mirror surface microstructure. With the optimized parameters, a 7.8 μm dense modified layer was generated, which was mainly attributed to the laser healing of micropits and unmolten particles.

4. On the laser modified surface of the mirror, the Sa value of surface roughness after chemical mechanical polishing was 3.7 nm, because the microscopic pores and unmolten particles were eliminated.

5. It is expected that the mirror surface fabricated in this study can satisfy the requirements for near-infrared or even visible applications. Moreover, the mirrors exhibited strong temperature stability, owing to the elimination of the bimetallic effect caused by the NiP layer.

Funding. National Natural Science Foundation of China (52175538, 62127901); Department of Science and Technology of Jilin Province (20210509067RQ).

Disclosures. The authors declare no conflicts of interest.

Data availability. Data underlying the results presented in this paper are not publicly available at this time but may be obtained from the authors upon reasonable request.

References

1. R. Steinkopf, A. Gebhardt, S. Scheiding, M. Rohde, O. Stenzel, S. Gliech, V. Giggel, H. Löscher, G. Ullrich, P. Rucks, A. Duparre, S. Risse, R. Eberhardt, and A. Tünnermann, "Metal mirrors with excellent figure and roughness," Proc. SPIE **7102**, 71020C–173 (2008).
2. S. Risse, A. Gebhardt, C. Damm, T. Peschel, W. Stöckl, T. Feigl, S. Kirschstein, R. Eberhardt, N. Kaiser, and A. Tünnermann, "Novel TMA telescope based on ultra precise metal mirrors," Proc. SPIE **7010**, 701016–372 (2008).
3. L. Gardner, "Metal additive manufacturing in structural engineering–review, advances, opportunities and outlook," Structures **47**, 2178–2193 (2023).
4. W. Wang and Y. Xia, "Topology optimization based channel design for powder-bed additive manufacturing," Addit. Manf. **54**, 102717 (2022).
5. Y. Wu, M. Li, J. Wang, Y. Wang, X. An, H. Fu, and Q. Zou, "Powder-bed-fusion additive manufacturing of molybdenum: Process simulation, optimization, and property prediction," Addit. Manf. **58**, 103069 (2022).
6. K. Zhang, X. Xie, C. Wang, H. Wang, F. Xu, H. Wang, and J. Zhang, "Optomechanical performances of advanced lightweight mirrors based on additive manufacturing," Micromachines **13**(8), 1334 (2022).
7. C. Weller, R. Kleer, and F. T. Piller, "Economic implications of 3D printing: Market structure models in light of additive manufacturing revisited," Int. J Prod. Econ. **164**, 43–56 (2015).
8. M. Brunelle, I. Ferralli, R. Whitsitt, and K. Medicus, "Current use and potential of additive manufacturing for optical applications," Proc. SPIE **10448**, 129–139 (2017).
9. M. Sweeney, M. Acreman, T. Vettese, R. Myatt, and M. Thompson, "Application and testing of additive manufacturing for mirrors and precision structures," Proc. SPIE **9574**, 47–59 (2015).
10. T. N. Lam, A. Lee, Y. R. Chiu, H. F. Kuo, T. Kawasaki, S. Harjo, and E. W. Huang, "Estimating fine melt pool, coarse melt pool, and heat affected zone effects on the strengths of additive manufactured AlSi10Mg alloys," Mater. Sci. Eng. **856**, 143961 (2022).
11. H. Liu, M. Ye, Z. Ye, L. Wang, G. Wang, X. Shen, and C. Wang, "High-quality surface smoothening of laser powder bed fusion additive manufacturing AlSi10Mg via intermittent electrochemical polishing," Surf. Coat. Technol. **443**, 128608 (2022).

Optics EXPRESS

12. C. Atkins, W. Brzozowski, N. Dobson, M. Milanova, S. Todd, D. Pearson, and I. T. Nistea, "Additively manufactured mirrors for CubeSats," Proc. SPIE **11116**, 41–352 (2019).
13. M. Roulet, C. Atkins, E. Hugot, S. Lemared, S. Lombardo, and M. Ferrari, "3D printing for astronomical mirrors," Proc. SPIE **10675**, 3 (2018).
14. T. Thoř, A. Procházková, F. Procháska, R. Doleček, M. Špína, J. Václavík, and M. Mulser, "Development of an ultraprecision metal mirror on additively manufactured Ti-6Al-4 V," Appl. Opt. **60**(31), 9919–9924 (2021).
15. Y. Wang, J. Yu, and Z. Wang, "Surface quality improvement at selective laser melting AlSi10Mg by optimizing single point diamond turning parameters," Mater. Test. **65**(1), 63–76 (2023).
16. P. Böttner, A. Brady, C. Reinlein, R. Eberhardt, and S. Nolte, "Design routine and characterisation of a biconic deformable metal mirror for focus shifting," Opt. Express **29**(3), 2971–2983 (2021).
17. E. Hilpert, J. Hartung, S. Risse, R. Eberhardt, and A. Tünnermann, "Precision manufacturing of a lightweight mirror body made by selective laser melting," Precis. Eng. **53**, 310–317 (2018).
18. H. Herzog, J. Segal, J. Smith, R. Bates, and R. Wicker, "Optical fabrication of lightweighted 3D printed mirrors," Proc. SPIE **9573**, 53–67 (2015).
19. J. Guo, X. Shi, C. Song, L. Niu, H. Cui, X. Guo, Z. Tong, N. Yu, Z. Jin, and R. Kang, "Theoretical and experimental investigation of chemical mechanical polishing of W-Ni-Fe alloy," Int. J. Extrem. Manuf. **3**(2), 025103 (2021).
20. L. Yan, X. Zhang, Q. Fu, L. Wang, G. Shi, and S. Tan, "Assembly-level topology optimization and additive manufacturing of aluminum alloy primary mirrors," Opt. Express **30**(4), 6258–6273 (2022).
21. E. Hilpert, J. Hartung, H. V. Lukowicz, T. Herffurth, and N. Heidler, "Design, additive manufacturing, processing, and characterization of metal mirror made of aluminum silicon alloy for space applications," Opt. Eng. **58**(09), 1 (2019).
22. M. Roulet, C. Atkins, E. Hugot, R. Snell, and H. Schnelter, "Use of 3D printing in astronomical mirror fabrication," Proc. SPIE **11349**, 15–44 (2020).
23. D. Kang, P. Zou, H. Wu, W. Wang, and J. Xu, "Research on ultrasonic vibration-assisted laser polishing of the 304 stainless steel," J Manuf. Process **62**, 403–417 (2021).
24. Y. Ren and Z. Zhang, "Formation mechanism of nanosecond-laser-induced microstructures on amorphous silicon film surfaces," Opt. Express **29**(21), 33804–33817 (2021).
25. A. E. Hassanin, M. A. Obeidi, F. Scherillo, and D. Brabazon, "CO_2 laser polishing of laser-powder bed fusion produced AlSi10Mg parts," Surf. Coat. Technol. **419**, 127291 (2021).
26. D. Zhang, J. Yu, H. Li, X. Zhou, C. Song, C. Zhang, S. Shen, L. Liu, and C. Dai, "Investigation of laser polishing of four selective laser melting alloy samples," Appl. Sci. **10**(3), 760 (2020).
27. S. Tan, Y. Ding, Y. Xu, and L. Shi, "Design and fabrication of additively manufactured aluminum mirrors," Opt. Eng. **59**(01), 1 (2020).
28. Y. Wang and J. Shi, "Effect of hot isostatic pressing on nanoparticles reinforced AlSi10Mg produced by selective laser melting," Mater. Sci. Eng., A **788**, 139570 (2020).
29. T. Hirata, T. Kimura, and T. Nakamoto, "Effects of hot isostatic pressing and internal porosity on the performance of selective laser melted AlSi10Mg alloys," Mater. Sci. Eng., A **772**, 138713 (2020).
30. P. A. Du and E. Macdonald, "Hot isostatic pressing in metal additive manufacturing: X-ray tomography reveals details of pore closure," Addit. Manf. **34**, 101191 (2020).
31. M. C. Kong, W. B. Lee, C. F. Cheung, and S. To, "A study of materials swelling and recovery insingle-point diamond cutting of ductile materials," J. Mater. Process. Technol. **180**(1-3), 210–215 (2006).
32. W. C. Oliver and G. M. Pharr, "An improved technique for determining hardness and elastic modulus using load and displacement sensing indentation experiments," J. Mater. Res. **7**(6), 1564–1583 (1992).